

Anisotropic universe with anisotropic sources

Pavan K. Aluri^{*}, Sukanta Panda[†], Manabendra Sharma[‡] and Snigdha Thakur[§]

Department of Physics, IISER Bhopal, Bhopal - 462023, India

Abstract

We analyze the state space of a Bianchi-I universe with anisotropic sources. Here we consider an extended state space which includes null geodesics in this background. The evolution equations for all the state observables are derived. Dynamical systems approach is used to study the evolution of these equations. The asymptotic stable fixed points for all the evolution equations are found. We also check our analytic results with numerical analysis of these dynamical equations. The evolution of the state observables are studied both in cosmic time and using a dimensionless time variable. Then we repeat the same analysis with a more realistic scenario, adding the isotropic (dust like dark) matter and a cosmological constant (dark energy) to our anisotropic sources, to study their co-evolution. The universe now approaches a de Sitter space asymptotically dominated by the cosmological constant. The cosmic microwave background anisotropy maps due to shear are also generated in this scenario, assuming that the universe contains anisotropic matter along with the usual (dark) matter and vacuum (dark) energy since decoupling. We find that they contribute dominantly to the CMB quadrupole. We also constrain the current level of anisotropy and also search for any cosmic preferred axis present in the data. We use the Union 2 Supernovae data to this extent. An anisotropy axis close to the mirror symmetry axis seen in the cosmic microwave background data from Planck probe is found.

1 Introduction

In standard cosmology it is assumed that the space-time is homogeneous and isotropic. After the discovery of temperature anisotropies of the Cosmic Microwave Background (CMB) and accelerating expansion of the universe, a standard cosmological model describing universe dominated by cold dark matter (CDM) and dark energy in the form of a cosmological constant (Λ) is formulated, known as Λ CDM model or cosmic concordance model. Fluctuations in the temperature of CMB radiation are statistically isotropic in this model [1]. A central assumption in our standard model of cosmology (and in most cosmological models) is that the universe is homogeneous and isotropic upto small perturbations, and thus described by a perturbed Friedmann-Robertson-Walker (FRW) metric. Observations show that the temperature of the CMB is isotropic to a remarkable degree indicating that our universe is close to a Friedmann-Lemaitre (FL) model. According to Ehlers, Geren and Sachs (EGS) theorem [2], if the CMB temperature were exactly isotropic about every point in space-time, then the universe has to be exactly an FL model. This result is not directly applicable to CMB, because, CMB radiation is not exactly isotropic. The presence of temperature anisotropies in the CMB from the observations made by COBE/WMAP satellites are inconsistent with an exact homogeneous and isotropic FRW model [3].

The current CMB data supports an inflationary Big Bang model of cosmic origin for our universe. However at large angular scales, there are some anomalies observed in CMB data, such as, a low value for quadrupole power, alignment of quadrupole and octopole modes roughly in the direction of Virgo cluster, ecliptic north-south power asymmetry, parity asymmetry between even and odd multipoles, almost zero correlations on large angular scales of CMB and an anomalous cold spot ($\sim 10^\circ$ diameter)

^{*}aluri@iucaa.ernet.in (Now at IUCAA, Pune - 411007, India)

[†]sukanta@iiserb.ac.in

[‡]manabendra@iiserb.ac.in

[§]snigdha@iiserb.ac.in

in the southern galactic hemisphere of the CMB sky [4]. Several solutions to these CMB anomalies have been put forth such as foregrounds/systematics, anisotropic space-times and exotic topologies [5]. Some of these supposed deviations seen in CMB data were addressed by the WMAP and Planck science teams also [6, 7]. These deviations may be an evidence that we live in a globally anisotropic universe.

Generally, in a global anisotropic universe, during inflation, shear decreases and eventually it goes over to an isotropic phase with negligible shear [8]. In order to produce any substantial amount of shear in recent times one needs to induce anisotropy in the space-time. One way to induce anisotropy is to have anisotropic matter present at the last scattering surface. It was shown earlier that the power suppression in CMB quadrupole, without affecting higher multipoles, can be explained by assuming anisotropic matter (magnetic fields) [9]. Earlier works on anisotropic cosmological models with anisotropic stresses can be found in Ref. [10]. Anisotropic dark energy as a possible solution to the cosmic acceleration as well as the large scale CMB anomalies is studied in Ref. [11]. The anisotropic sources can be a uniform magnetic field, cosmic strings or domain walls. A nanogauss scale magnetic field could be present today which would have been produced during inflation due to a Lorentz-violating term to the photon sector [12]. We call this as ‘‘Lorentz Violation generated magnetic field (LVMF)’’. Other possibilities such as a Maxwell type vector field coupled to a scalar field has been studied Ref. [13].

In this paper our approach is not to deal with metric approach directly, rather we adhere to an approach similar to orthonormal frame formalism [14]. The paper is organized as follows. In section 2, we write down the Einstein’s equations in cosmic time. Null geodesic equations in cosmic time are studied in section 3. In section 4, fixed point analysis of all the evolution equations is carried out in terms of a dimensionless time variable (τ), to study the asymptotic evolution of the state observables. A more realistic model including the ordinary dust like (dark) matter and a cosmological constant (dark energy) in addition to the anisotropic sources is considered in section 5. Then, in section 6, we show the temperature patterns for CMB due to co-evolution of individual anisotropic sources along with isotropic matter and vacuum energy. In section 7, we obtain constraints on the fractional energy densities of various components of the realistic model described earlier, the level of shear, and also determine a cosmic preferred axis if present. Finally, in section 8, we conclude our work.

2 Bianchi-I universe

In our approach to study dynamical systems, we formulate the evolution equations in terms of few dimensionless state observables. It is a very invaluable tool to obtain qualitative information about the solutions of the state space of Bianchi universes (see Ref. [14] and references therein). Here we concentrate only on Bianchi-I model. First we derive the Einstein’s equations in metric approach. Then we write them in terms of state observables analogous to the orthonormal frame formalism [15]. In this approach one writes the field equations as first order differential equations. An advantage of this orthonormal frame approach is that the derivation of geodesic equation is easy compared to the metric approach.

We start with a Bianchi-I line element with a residual planar symmetry in the yz -plane as

$$ds^2 = dt^2 - a(t)^2 dx^2 - b(t)^2 (dy^2 + dz^2). \quad (1)$$

We choose the diagonal energy momentum tensor of the form $T_\nu^\mu = (\rho, -p_a, -p_b, -p_b)$, where $p_a = w_a \rho$ and $p_b = w_b \rho$. The four kinds of anisotropic matter we study here are given in Table [1]. The magnetic field configuration considered here as an anisotropic source is well known [10]. We, then consider anisotropic matter configurations due to topological defects such as cosmic strings and domain walls. The energy-momentum tensors corresponding to these sources are given in appendix A. Finally, a magnetic field generated due to a Lorentz-violating term in the photon sector, abbreviated as LVMF, is also studied as an anisotropic source [12]. Here we assume that all these sources are of primordial origin and were produced through breaking of discrete symmetries during phase transitions in the early universe. A distribution of cosmic strings and domain walls may quickly grow anisotropic. We analyse them towards our motivation to study the anisotropic sources and their (asymptotic) evolution, and co-evolution with the (dust like) dark matter and dark energy (Λ), relevant at late times. Eventually we also obtain constraints on these anisotropic sources using Type Ia supernova data.

Matter	w_a	w_b
Cosmic String	-1	0
Domain Walls	0	-1
LVMF	1	0
Magnetic Field	-1	1

Table 1: Equation of state parameters for different anisotropic sources considered in this paper.

The Einstein's equations for the metric given in Eq. [1] are

$$\begin{aligned}
2H_a H_b + H_b^2 &= 8\pi G \rho, \\
2\dot{H}_b + 3H_b^2 &= -8\pi G p_a, \\
\dot{H}_a + \dot{H}_b + H_a^2 + H_a H_b + H_b^2 &= -8\pi G p_b,
\end{aligned} \tag{2}$$

where $H_a = \frac{1}{a} \frac{da}{dt}$ and $H_b = \frac{1}{b} \frac{db}{dt}$. The equation of continuity is given by,

$$\dot{\rho} + (H_a + 2H_b)\rho + H_a p_a + 2H_b p_b = 0. \tag{3}$$

Here onwards we choose to set $8\pi G = 1$ for the rest of this paper. This can otherwise be seen as rescaling, all the quantities in Eq. [2] with $1/\sqrt{8\pi G}$. Now, we rewrite the above set of equations, Eq. [2] and [3], in terms of the average expansion $H = (H_a + 2H_b)/3$ and shear $h = (H_b - H_a)/\sqrt{3}$. The Einstein's equations and the equation of continuity in cosmic time become

$$\begin{aligned}
\frac{dH}{dt} &= -H^2 - \frac{2}{3}h^2 - \frac{1}{6}(\rho + p_a + 2p_b), \\
\frac{dh}{dt} &= -3Hh + \frac{1}{\sqrt{3}}(p_b - p_a), \\
\frac{d\rho}{dt} &= -3H\left(\rho + \frac{p_a + 2p_b}{3}\right) - \frac{2h}{\sqrt{3}}(p_b - p_a),
\end{aligned} \tag{4}$$

and a constraint equation given by

$$H^2 = \frac{\rho}{3} + \frac{h^2}{3}. \tag{5}$$

We now introduce dimensionless variables H' , h' , t' defined as

$$\begin{aligned}
H' &= \frac{H}{H_0}, \\
h' &= \frac{h}{h_0}, \\
t' &= tH_0, \\
\rho' &= \frac{\rho}{\rho_0},
\end{aligned} \tag{6}$$

where H_0 , h_0 and ρ_0 are the current values of Hubble, shear and anisotropic matter density parameters, respectively. Then, the equations for the state observables in terms of these dimensionless variables can be written as

$$\begin{aligned}
\dot{H}' &= -H'^2 - \frac{2}{3}\left(\frac{h_0}{H_0}\right)^2 h'^2 - \frac{1}{2}(1 + w_a + 2w_b)\Omega_0 \rho', \\
\dot{h}' &= -3H'h' + \sqrt{3}(w_b - w_a)\frac{H_0}{h_0}\Omega_0 \rho', \\
\dot{\rho}' &= -3\left(1 + \frac{w_a + 2w_b}{3}\right)H'\rho' - \frac{2(w_b - w_a)}{\sqrt{3}}\frac{h_0}{H_0}h'\rho',
\end{aligned} \tag{7}$$

where an overdot represents differentiation with respect to t' and $\Omega_0 = \rho_0/3H_0^2$. Now, we solve the above equations numerically for all the cases listed in Table [1]. The evolution of the dynamic variables

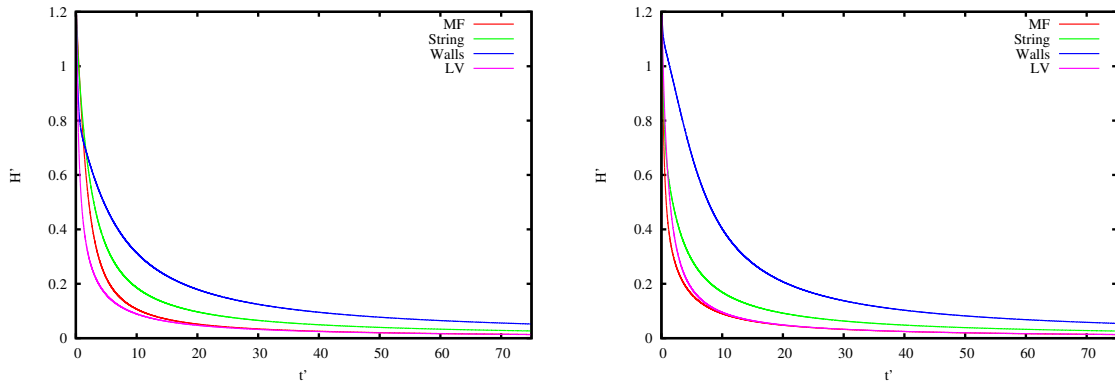


Figure 1: H' vs. t' . In the *left* figure, $h'(0) = 173$, $h_0/H_0 = 0.01$, $\Omega_0 = 0.1$, $\rho'(0) = 10$, and in the *right* figure $h'(0) = -173$, $h_0/H_0 = 0.01$, $\Omega_0 = 0.1$, $\rho'(0) = 10$.

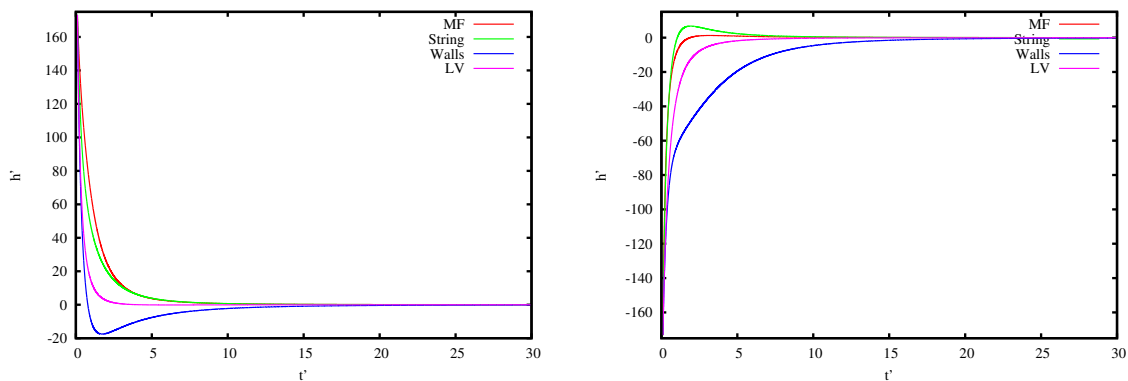


Figure 2: h' vs. t' . In the *left(right)* figure, the initial data is same as in *left(right)* figures of Fig. [1].

H' , h' and ρ' are plotted in Fig. [1], [2] and [3]. For all these anisotropic matter sources, it turns out that H' decreases with increasing time t' . Uniform magnetic field and LVMF matter have almost similar rate of expansion, whereas walls and strings have a higher rate of expansion. From Fig. [2], shear becomes negligible at late times and it decreases slowly for walls compared to the other three sources. Isotropy appears to set in at late times for all cases of anisotropic matter. A fixed point analysis will shed some light on the actual evolution. Detailed inspection of attaining isotropy at late times will be done in section 4. We observe from Fig. [3] that, the energy density also decreases much faster for magnetic field, LVMF and strings compared to walls.

From Fig. [2], it can be observed that evolution of shear depends on the initial conditions. Signature change of shear can be seen for certain kind of anisotropic matter. This signature change may have implications in early universe. From the left plot of Fig. [2], we see that this change occurs for walls, whereas the right plot of Fig. [2] shows a similar signature change but for cosmic strings, depending on a positive/negative shear in the beginning. However late time behaviour of H' , h' and ρ' in cosmic time are independent of initial conditions for all these sources.

3 Null Geodesic evolution

As we know the geodesic equations are second order differential equations in metric approach. If we represent the same equation in terms of H and h , then the geodesics can be written as first order differential equations given by [16]

$$\begin{aligned} \frac{d\epsilon}{dt} &= -H\epsilon - \frac{(\epsilon^2 - 3k_1^2)h}{\sqrt{3}\epsilon}, \\ \frac{dk_1}{dt} &= \left(-H + \frac{2h}{\sqrt{3}}\right)k_1, \end{aligned}$$

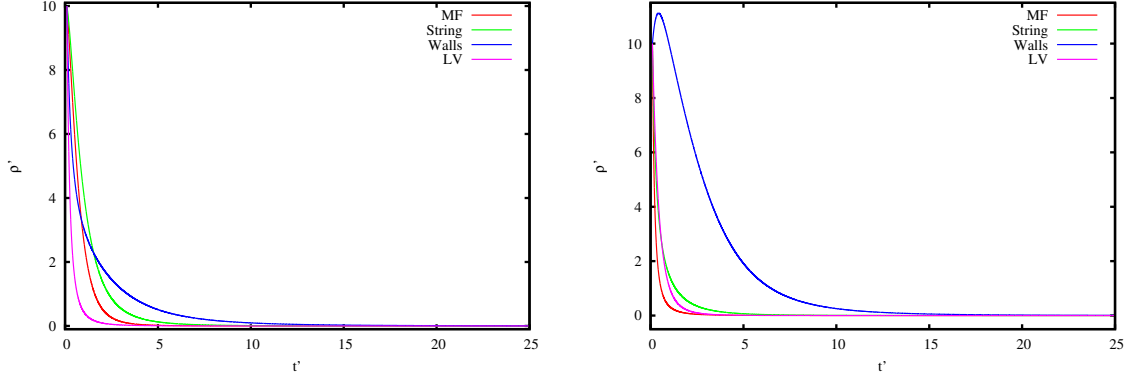


Figure 3: ρ' vs. t' . In the *left(right)* figure, the initial data is same as in *left(right)* figures of Fig. [1].

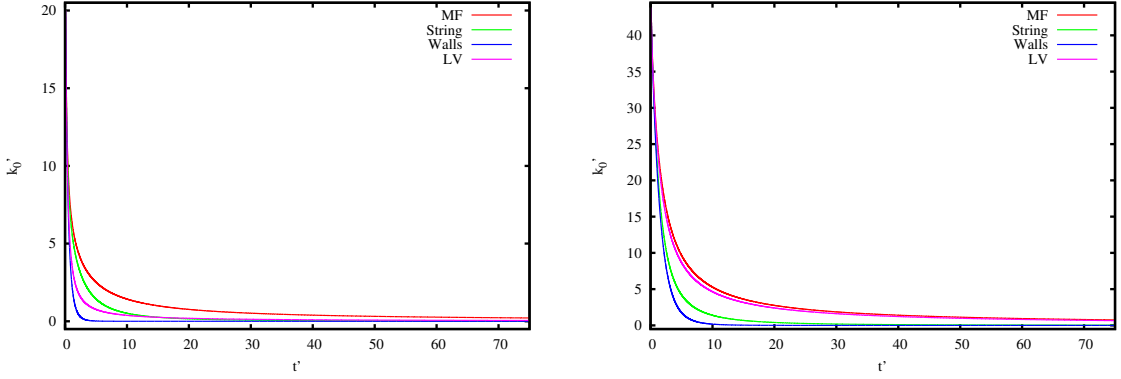


Figure 4: k_0 vs. t' . The initial data is same as in Fig. [1] with $\epsilon(0) = k_0 = 20$ (*left* - Case 1) and, $\epsilon(0) = k_0 = 20$ and $k_1(0) = k_3(0) = 25.3$ (*right* - Case 2).

$$\begin{aligned} \frac{dk_2}{dt} &= \left(-H - \frac{h}{\sqrt{3}}\right) k_2, \\ \frac{dk_3}{dt} &= \left(-H - \frac{h}{\sqrt{3}}\right) k_3, \end{aligned} \quad (8)$$

where $\epsilon = k_0$ is the energy of photon, and k_1, k_2 and k_3 are the three components of photon momentum (\vec{k}). The variables ϵ and k_i ($i=1,2,3$) satisfies the constraint equation

$$\epsilon^2 = |\vec{k}|^2. \quad (9)$$

In terms of cosmic time t' the above equations become

$$\begin{aligned} \dot{\epsilon} &= -H'\epsilon - \frac{h_0}{H_0} \frac{(\epsilon^2 - 3k_1^2)h'}{\sqrt{3}\epsilon}, \\ \dot{k}_1 &= \left(-H' + 2\frac{h_0}{H_0} \frac{h'}{\sqrt{3}}\right) k_1, \\ \dot{k}_2 &= \left(-H' - \frac{h_0}{H_0} \frac{h'}{\sqrt{3}}\right) k_2, \\ \dot{k}_3 &= \left(-H' - \frac{h_0}{H_0} \frac{h'}{\sqrt{3}}\right) k_3, \end{aligned} \quad (10)$$

where an overdot here represents differentiation with respect to t' .

In order to solve the null geodesics, Eq. [10], one needs to take care that the solutions simultaneously satisfy the constraint equation, Eq. [9]. We solve these geodesic equations numerically for the following two cases.

Case 1 : In this case only k_1 is taken to be nonzero, and k_2 and k_3 are zero. Initial values are taken

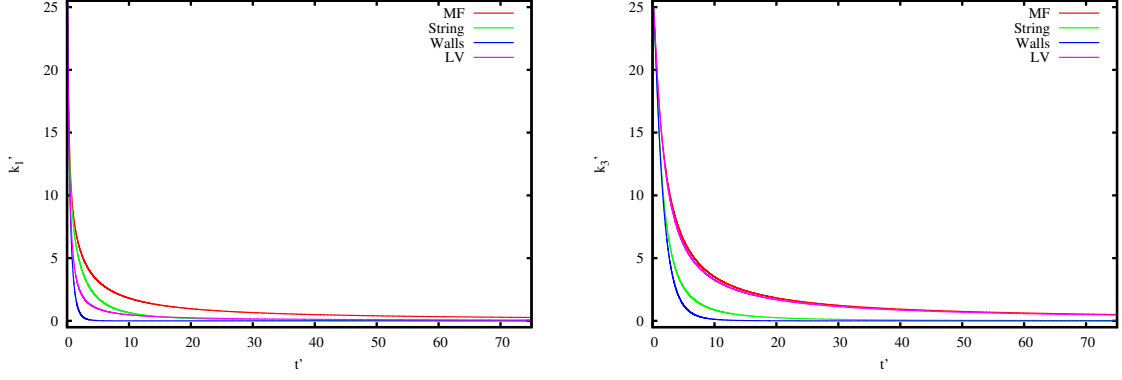


Figure 5: Shown here are k_1 vs. t' (left) and k_3 vs. t' (right). The initial data is same as in Fig. [1] except for $k_1(0) = k_3(0) = 25.3$. These plots correspond to Case 2.

as $k_0(0) = 20$ and $k_2(0) = k_3(0) = 0$. The constraint equation, Eq. [9], gives $k_1 = \pm k_0 = \pm \epsilon$. Here we choose the positive value for k_1 . The evolution of k_0 is shown in the left plot of Fig. [4] for an initial values of $k_0(0) = 20$, for the four anisotropic sources we are considering. Here we find that, if the initial value of k_1 is positive then for the entire evolution it remains positive. It's also true for negative initial values of k_1 , where it remains negative for the whole evolution. Other initial values are same as those of Fig. [1], [2] and [3]. We observe that k_0 decreases slowly for magnetic field and faster for walls. This can be understood from Fig. [1] where H' decreases slowly for walls and faster for a magnetic field.

Case 2: In this case we take $k_1(0) = k_3(0) = 25.3$ and, $k_2 = k_3$ following the residual planar symmetry of our metric. Other initial values are same as Case 1. The evolution of k_0 is shown in the right plot of right plot of Fig. [4], and k_1 and k_3 are shown in Fig. [5]. Here also, we observe that k_0 decreases slowly for magnetic field and faster for walls. k_1 and k_3 also evolve in a similar manner, except for the interchange of evolution of cosmic strings and LVMF.

4 Fixed point analysis of the evolution equations

In the previous section, we studied the evolution of state observables in terms of a time variable analogous to cosmic time. In order to study the asymptotic evolution of our Bianchi-I universe with various anisotropic sources considered here, we resort to dynamical systems approach. So, we cast all the evolution equations in terms of dimensionless variables which give us a set of dynamical equations. The advantage of working in this approach is that we can show the cosmological dynamics insensitive to the initial conditions. Here we define the dimensionless variables τ and σ as $d\tau/dt = H$ and $\sigma = h/\sqrt{3}H$, respectively. These are called expansion normalized time and shear variables. Thus our Einstein's equations and the continuity equation are given by

$$\begin{aligned} \frac{dH}{d\tau} &= -H(1+q), \\ \frac{d\sigma}{d\tau} &= \frac{3}{2} \left[-\sigma(1-\sigma^2) + \left(\frac{2(w_b - w_a)}{3} + w\sigma \right) \Omega \right] \end{aligned} \quad (11)$$

and

$$\Omega + \sigma^2 = 1, \quad (12)$$

where $q = 2\sigma^2 + (1+2w)\Omega/2$, $w = (w_a + 2w_b)/3$ and $\Omega = \rho/3H^2$.

Next, we write the null geodesic equations in terms of dimensionless variables $K_i = k_i/k_0$ ($i=1,2,3$). They are given by

$$\begin{aligned} \frac{d\epsilon}{d\tau} &= -(1+s)\epsilon, \\ \frac{dK_1}{d\tau} &= (s+2\sigma)K_1, \end{aligned}$$

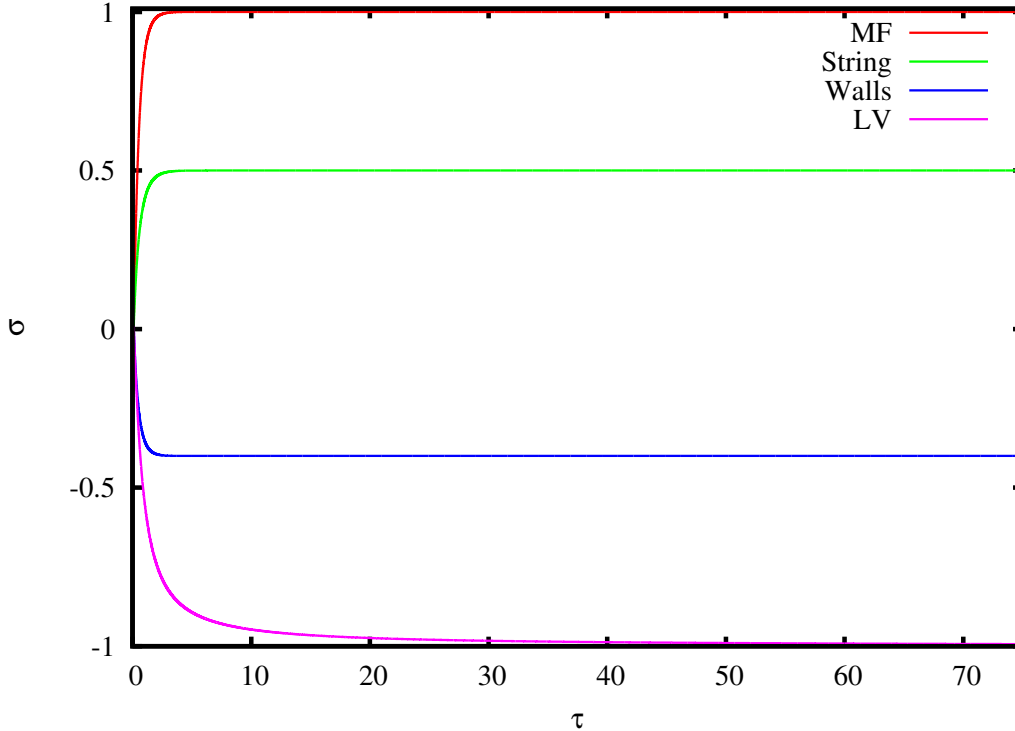


Figure 6: σ vs τ : Late time behaviour of σ for each of the four anisotropic matter sources considered separately, are shown here.

$$\begin{aligned}\frac{dK_2}{d\tau} &= (s - \sigma)K_2, \\ \frac{dK_3}{d\tau} &= (s - \sigma)K_3,\end{aligned}\tag{13}$$

where $s = (1 - 3K_1^2)\sigma$. The variables K_i ($i=1,2,3$) satisfy the constraint equation

$$|\vec{K}|^2 = 1.\tag{14}$$

Now, we will analyze the fixed points of the full set of equations combining Einstein's equations, equation of continuity and the null geodesic equations [16]. Fixed points for σ can be easily obtained from Eq. [11], which are ± 1 and $2(w_b - w_a)/3(1 - w)$. From Eq. [13], we have $K_1 = \pm 1$ and $K_2 = 0$ or $K_1 = 0$ and $K_2 = \pm 1/\sqrt{2}$, as implied by Eq. [14], as fixed points. All the stable fixed points are given in Table [2]. Detailed evaluation of stable fixed points is given in appendix B. Same conclusion can be drawn from solving these equations numerically. The evolution of σ and, K_1 and K_3 are plotted in Fig. [6] and [7]. Asymptotically, we can see that σ , K_1 and K_3 evolve towards their corresponding stable fixed points. We now clearly see that isotropy can't be attained at late times for any of the anisotropic sources, considered here, through this fixed point analysis. This is in contrast to what *appeared* to be the case studying the physical variables themselves in the preceding sections. This is one of the advantages of such an analysis. One may not draw a similar conclusion from our analysis done in cosmic time. This whole evolution depends on the positive or negative initial values of K_1 and K_3 . Once we choose positive initial value for K_1 and K_3 , then it remains positive for the whole evolution. Similarly it stays negative for the whole evolution if negative initial values are chosen.

Kasner solutions

Exact solutions of Kasner type can be obtained for the Einstein's equations corresponding to the fixed points of the shear parameter σ [17]. In order to find Kasner type solution at stable fixed points we choose scale factors as $a(t) = At^\alpha$ and $b(t) = Bt^\beta$, where A and B are some positive constants. For

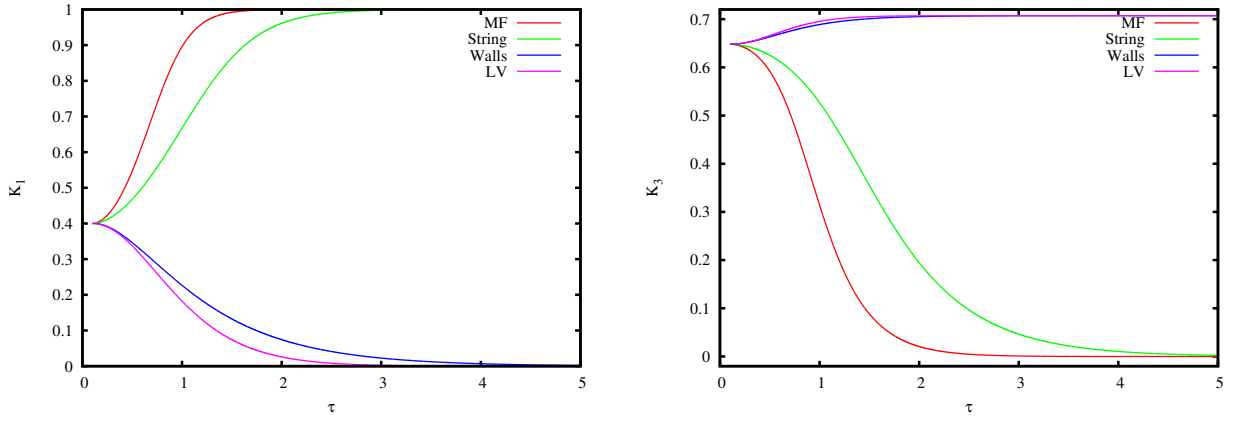


Figure 7: Evolution of K_1 vs. τ (*left*), and K_3 vs. τ (*right*) are shown here for the various anisotropic matter sources. Here an initial value of $\sigma = 0.01$ is used.

Matter	σ_0	(K_1^0, K_2^0, K_3^0)
Cosmic String	1/2	$(\pm 1, 0, 0)$
Domain Walls	-2/5	$(0, \pm 1/\sqrt{2}, \pm 1/\sqrt{2})$
LVMF	-1	$(0, \pm 1/\sqrt{2}, \pm 1/\sqrt{2})$
Magnetic Field	1	$(\pm 1, 0, 0)$

Table 2: Stable fixed points of the whole state space of a Binachi I universe for different anisotropic matter sources.

these scale factors, we can write the evolution equations as

$$\begin{aligned} H_a &= H(1 - 2\sigma) \\ H_b &= H(1 + \sigma) \end{aligned} \quad (15)$$

and average scale factor H satisfies

$$\frac{dH}{dt} = -(1 + q)H^2. \quad (16)$$

After substituting the power law form for the scale factors into Eq. [15] and [16] and solving, we get

$$\alpha = \frac{1 + 2\sigma}{1 + q}, \quad \beta = \frac{1 - \sigma}{1 + q}. \quad (17)$$

The Kasner solutions are summarized in Table [3]. From the exact solutions we observe that in the case of cosmic strings, universe accelerates in one direction and decelerates in the other two directions. Then, in the case of domain walls, it decelerates in one direction and accelerates in the other two directions. For LVMF, it contracts in one direction and decelerates in the other two directions, and for magnetic fields, universe expands along only one dimension, while it's static in the other two dimensions.

5 A more realistic scenario

In this section we extend our analysis of the previous section by adding the usual dust like dark matter and cosmological constant as dark energy to our anisotropic matter types, in order to make it a realistic

Matter	σ_0	α	β
Cosmic String	1/2	4/3	1/3
Domain Walls	-2/5	2/9	14/9
LVMF	-1	-1/3	2/3
Magnetic Field	1	1	0

Table 3: Kasner type solutions at the asymptotic stable fixed points of the state space variables.

scenario, relevant for the current evolution of our universe. We do our analysis in τ -time which is useful to find stable fixed points. However, the form of the geodesic equations will be unchanged. Here we analyse the asymptotic evolution numerically.

The evolution equations in τ -time for this model which includes anisotropic matter, isotropic (dust like) dark matter and dark energy (Λ) are given by

$$\begin{aligned}
\frac{dH}{d\tau} &= -(1+q)H, \\
q &= 2\sigma^2 + \frac{1}{2}[\Omega_{IM}(1+3w_{IM}) + \Omega_{AM}(1+3w_{AM}) + \Omega_{\Lambda}(1+3w_{\Lambda})], \\
\frac{d\sigma}{d\tau} &= (1+q)\sigma - 3\sigma + (w_b - w_a)\Omega_{AM}, \\
\frac{d\Omega_{IM}}{d\tau} &= 2(1+q)\Omega_{IM} - 3(1+w_{IM})\Omega_{IM}, \\
\frac{d\Omega_{\Lambda}}{d\tau} &= 2(1+q)\Omega_{\Lambda}, \\
\Omega_{AM} &= 1 - (\Omega_{IM} + \Omega_{\Lambda} + \sigma^2),
\end{aligned} \tag{18}$$

where,

$$\begin{aligned}
w_{IM} &= 0, \\
w_{\Lambda} &= -1, \\
w_{AM} &= (w_a + 2w_b)/3, \\
p_{IM} &= w_{IM}\rho_{IM}, \\
p_{\Lambda} &= w_{\Lambda}\rho_{\Lambda}, \\
p_{AM}^i &= w_{AM}^i\rho_{AM}, \quad i = a, b \\
\sigma &= h/\sqrt{3}H, \\
\Omega_i &= \rho_i/3H^2, \quad i = IM, \Lambda, AM.
\end{aligned}$$

The evolution of $\sigma, \Omega_{IM}, \Omega_{\Lambda}$ and Ω_{AM} are given in Fig. [8] for the two cases $\Omega_{IM} > \Omega_{AM}$ and $\Omega_{IM} < \Omega_{AM}$. The late time behaviour in all these cases is almost same except for domain walls. However small may be the value of Ω_{DW} to start with, it turns out that Ω_{DW} tends to rise at intermediate times, and can even dominates over isotropic matter at present time for some initial values. This may not be a viable scenario as we know that the current dominant matter content is of isotropic type. However the other anisotropic sources can give rise to a viable scenario. For the actual evolution of an initial ordinary (isotropic dark) matter dominated era with small fractions of anisotropic matter and shear, to the current era of dark energy domination, the deceleration parameter is found to evolve from 1/2 to -1 at late times, as expected.

6 Temperature Patterns

For a Bianchi-I universe with anisotropic matter, along with the usual (isotropic) dark matter and dark energy (Λ), we find the contribution to the CMB temperature anisotropies due to these sources here. It has been shown earlier that the total quadrupole anisotropy in the presence of a uniform magnetic field, can be small compared to that obtained from the standard Λ CDM model [9]. The temperature of the cosmic microwave background as a function of the angular coordinates $\hat{n} = (\theta, \phi)$ on the celestial sphere is given by [18],

$$T(\theta, \phi) = T_{LSS} \exp \left[- \int_{\tau_{LSS}}^{\tau_0} (1+p) d\tau \right] \tag{19}$$

where T_{LSS} is the mean isotropic temperature of the CMB at the surface of last scattering, and

$$p = \Sigma_{\alpha\beta} K^{\alpha} K^{\beta}. \tag{20}$$

The direction cosines along a null geodesic K^{α} in terms of the spherical polar angles (θ, ϕ) are given by

$$K^{\alpha}(\tau_0) = (\cos \theta, \sin \theta \cos \phi, \sin \theta \sin \phi). \tag{21}$$

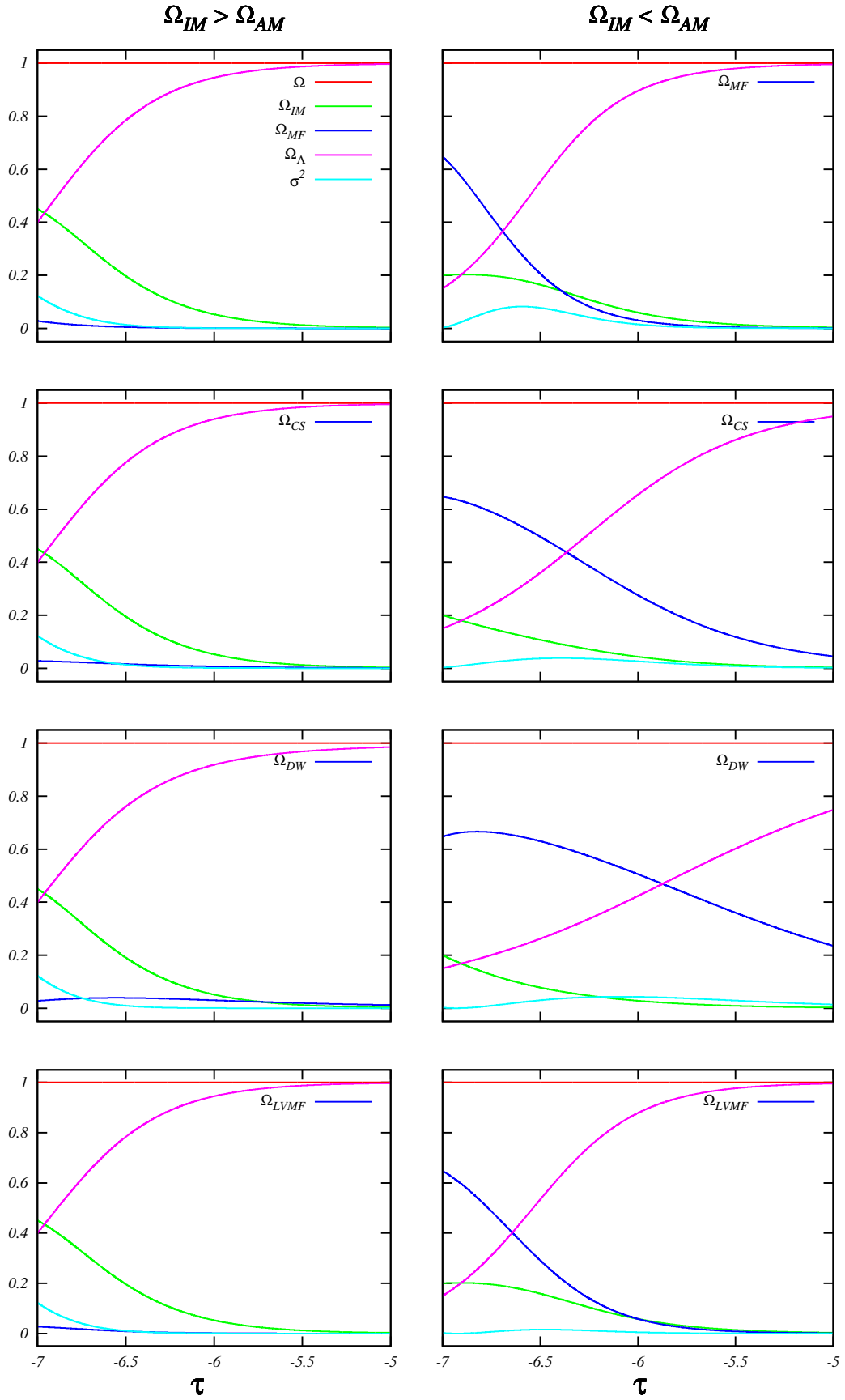


Figure 8: Ω vs τ : Late time behaviour of shear and density fractions of Λ CDM components in addition to the individual anisotropic sources studied in this work. Some representative initial values were used for the two cases of $\Omega_{IM} > \Omega_{AM}$ (left column) and $\Omega_{IM} < \Omega_{AM}$ (right column). The evolution shown here is from $\tau_{LSS} = -7$ to $\tau_0 = 0$ (today).

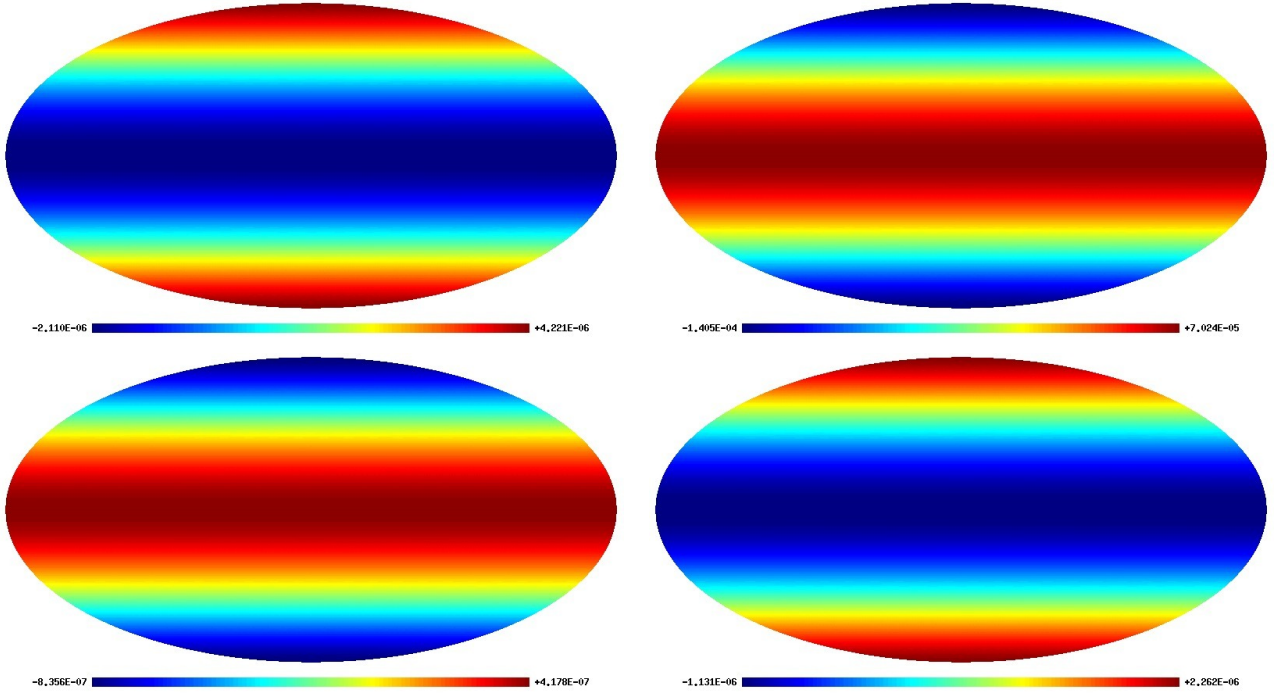


Figure 9: Temperature patterns $T(\theta, \phi)/T_{LSS}$ for Cosmic Strings (*top left*), Domain walls (*top right*), LVMF (*bottom left*) and Magnetic field (*bottom right*). Here we used $\sigma_{LSS} = 10^{-8}$ for CS and DW, and $\sigma_{LSS} = 10^{-5}$ for LVMF and MF.

In our case of planar geometry, $\Sigma_{\alpha\beta}$ takes the form

$$\Sigma_{\alpha\beta} = \text{diag}(-2\sigma, \sigma, \sigma). \quad (22)$$

Substituting Eq. [21] and [22] into Eq. [20] we get

$$p = (1 - 3K_1^2)\sigma. \quad (23)$$

The geodesic equation for K_1 is

$$\frac{dK_1}{d\tau} = 3(1 - K_1^2)K_1\sigma, \quad (24)$$

Using Eq. [23] and [24] in Eq. [19], we get

$$T(\theta, \phi) = T_{LSS} \frac{e^{\tau_{LSS} - \tau_0} e^{2\zeta_0}}{\sqrt{e^{6\zeta_0} + (1 - e^{6\zeta_0}) \cos^2 \theta}}, \quad (25)$$

where τ_0 ($= 0$) and τ_{LSS} ($= -7$) are the values of τ - today and at the time of decoupling, respectively - and

$$\zeta_0 = \int_{\tau_{LSS}}^{\tau_0} \sigma d\tau. \quad (26)$$

It turns out that the contribution is dominant to quadrupole for all the four cases of anisotropic matter types considered here. The CMB quadrupole temperature patterns are shown in Fig. [9]. We find that all other higher multipoles receive negligible contribution from these sources. Hence we only show temperature patterns for $l = 2$ here. There could be a dipole anisotropy also in CMB due to spatially inhomogeneous and anisotropy spaces such as, for example, in Ref. [19]. But, since our matter types are comoving sources and do not have peculiar motion, we do not see a dipole contribution to CMB anisotropies due to these sources. We also observe from Fig. [9] that the temperature maps for magnetic field and cosmic strings have similar patterns, whereas temperature maps for domain walls and LVMF show similar patterns. This has to do with the signature of ζ_0 , which in turn is related to σ (see Fig. [6]).

7 SN Ia constraints on cosmic shear and anisotropy

In this section, we will test our anisotropic Bianchi-I model with anisotropic sources using supernova data. We constrain the level of anisotropic matter density, shear, and also determine the cosmic preferred axis, if present, in addition to the current Hubble parameter, cold dark matter and dark energy (modeled as cosmological constant) density fractions, using the Type Ia supernova (SN1a) objects in the Union 2 compilation [20]¹ For this section, we use the evolution equations as determined from the line element

$$ds^2 = dt^2 - a^2(dx^2 + dy^2) - b^2dz^2 \quad (27)$$

which corresponds to the frame where the anisotropy axis is along the z -direction. Thus, the mean scale factor and the eccentricity are given by

$$\begin{aligned} A &= (a^2b)^{1/3} \\ e^2 &= 1 - \frac{b^2}{a^2}. \end{aligned} \quad (28)$$

The redshift (z) and luminosity distance (d_L) of an SN1a object observed in the direction $\hat{n} = (\theta, \phi)$ are given by [11]

$$1 + z(\hat{n}) = \frac{1}{A} \frac{(1 - e^2 \sin^2 \alpha)^{1/2}}{(1 - e^2)^{1/3}}, \quad (29)$$

and

$$d_L(\hat{n}) = c(1 + z) \int_{A(z)}^1 \frac{dA}{A^2 H} \frac{(1 - e^2)^{1/6}}{(1 - e^2 \cos^2 \alpha)^{1/2}}, \quad (30)$$

where α is the angle between the cosmic preferred axis ($\hat{\lambda}$) and the supernova position (\hat{n}), and ‘ c ’ is the speed of light. Hence, $\cos \alpha = \hat{\lambda} \cdot \hat{n}$. In order to obtain constraints on our Bianchi-I model with anisotropic matter and shear in addition to Λ CDM components, we fit the measured distance modulus of various SN1a objects that are provided in the Union 2 compilation to the theoretical distance modulus, by minimizing the χ^2 defined as

$$\chi^2 = \sum_i \frac{(\mu_i^d - \mu_i^{th})^2}{(\delta\mu_i^d)^2}, \quad (31)$$

where μ_i^d is the measured distance modulus of an SN1a object from data, μ_i^{th} is the theoretical distance modulus function involving various cosmological parameters, $\delta\mu_i^d$ is the measured uncertainty in the distance modulus of an SN1a object provided in the data, and the summation is over all SN1a objects of the data (total 557 supernovae).

The theoretical distance modulus is defined as

$$\mu^{th} = 5 \log \left(\frac{d_L}{10pc} \right), \quad (32)$$

where pc in the denominator stands for ‘parsec’, and d_L is the luminosity distance defined in Eq. [30]. By using the parametrization $H = 100 h \text{ Km.sec}^{-1}/\text{Mpc} = k h$, where k is dimensionfull and h being the dimensionless Hubble parameter, Eq. [32] can be further simplified to give

$$\mu^{th} = 5 \log \tilde{d}_L + 5 \log \left(\frac{c/k}{10^{-5} \text{ Mpc}} \right) = 5 \log \tilde{d}_L + \mu_0, \quad (33)$$

where $\mu_0 = 42.384$, and \tilde{d}_L , containing dimensionless quantities, is given by

$$\tilde{d}_L(\hat{n}) = (1 + z) \int_{A(z)}^1 \frac{dA}{A^2 h} \frac{(1 - e^2)^{1/6}}{(1 - e^2 \cos^2 \alpha)^{1/2}}. \quad (34)$$

¹The positions of the supernovae are in part obtained from <http://vizier.u-strasbg.fr>, <http://www.cbat.eps.harvard.edu/lists/Supernovae.html> and http://sdssdp62.fnal.gov/sdsssn/snlist_confirmed_updated.php web pages.

In this section, we use ‘ h ’ to denote the dimensionless Hubble parameter. The luminosity distance, \tilde{d}_L , (and thus the distance modulus μ) depends on all the cosmological parameters $\{h_0(\equiv H_0), \sigma_0, \Omega_0^{AM}, \Omega_0^{IM}, \Omega_0^\Lambda, \hat{\lambda} = (l_A, b_A)\}$. The minimization is done in conjugation with solving the evolution equations

$$\begin{aligned}
\frac{dA}{dz} &= \frac{-f_1}{(1+z)(1+z-f_1 f_2 \frac{\sigma}{A})} \\
f_1 &= \frac{(1-e^2 \sin^2 \alpha)^{1/2}}{(1-e^2)^{1/3}} \\
f_2 &= \frac{2+(e^2-3)\sin^2 \alpha}{1-e^2 \sin^2 \alpha} \\
(e^2)' &= \frac{6\sigma}{A}(1-e^2) \\
\frac{h'}{h} &= -\frac{3}{2}(1+\sigma^2+\bar{w}\Omega_{AM}-\Omega_\Lambda) \\
\sigma' &= -\frac{3}{2}\left(\sigma(1-\sigma^2)-\left(\frac{2}{3}\delta_w+\bar{w}\sigma\right)\Omega_{AM}+\sigma\Omega_\Lambda\right) \\
\Omega'_{AM} &= -3\Omega_{AM}\left(\bar{w}+\frac{2}{3}\delta_w\sigma-\bar{w}\Omega_{AM}+\Omega_\Lambda-\sigma^2\right) \\
\Omega'_{IM} &= 3\Omega_{IM}\left(\bar{w}\Omega_{AM}-\Omega_\Lambda+\sigma^2\right) \\
\Omega'_\Lambda &= 3\Omega_\Lambda\left(1+\bar{w}\Omega_{AM}-\Omega_\Lambda+\sigma^2\right)
\end{aligned} \tag{35}$$

where $\bar{w} = (2w_a + w_b)/3$, $\delta_w = w_a - w_b$, σ is the shear and $\Omega_{AM}, \Omega_{IM}, \Omega_\Lambda$ are the fractional energy densities due to anisotropic matter (AM), ordinary isotropic dark matter (IM) and the dark energy (Λ). The ‘ $'$ ’ denotes a derivative with respect to ‘ τ ’. The mean scale factor ‘ A ’ and τ -time are related by $dA/d\tau = A$. These equations are evolved from $z = [0, z_i^{SN}]$ for each supernova i with the initial conditions at $z = 0$ as $A = 1$, $e = 0$ corresponding to the choice $a_0 = 1$ and $b_0 = 1$, and random guess values for the parameters $\{h_0, \sigma_0, \Omega_0^{AM}, \Omega_0^{IM}, \Omega_0^\Lambda, \hat{\lambda}\}$ to do the χ^2 minimization. The deceleration parameter is given by $q_0 = h'/h|_{z=0}$. These anisotropic matter source models in a Bianchi-I universe are compared with the standard concordance model using the luminosity distance relation given by

$$\tilde{d}_L = (1+z) \int_0^{z^{SN}} \frac{dz}{\sqrt{\Omega_0^{IM}(1+z)^3 + \Omega_0^\Lambda}}, \tag{36}$$

where $\Omega^{IM} + \Omega^\Lambda = 1$.

The results from supernovae distance modulus fits to the models with individual anisotropic sources in addition to cold dark matter and Λ , and for the model with standard Λ CDM components alone, are given in Table [4]. The corresponding χ^2 near it’s minimum as a function of the cosmological parameters in our anisotropic model, and only the Λ CDM parameters are shown in Fig. [10], [11] and [12]. In those figures, note that the χ^2 is shown only for the effective six parameters $\{h_0, \sigma_0, \Omega_0^{AM}, \Omega_0^\Lambda, \hat{\lambda} = (l_A, b_A)\}$ of our anisotropic model with individual anisotropic sources along with the standard model components in a Bianchi-I background, and the two Λ CDM parameters $\{h_0, \Omega_0^\Lambda\}$ corresponding to the flat FRW universe with the usual cold dark matter and dark energy, respectively. The ordinary isotropic matter (Ω_{IM}), is treated as dependent quantity in both the cases that can be estimated from the corresponding constraint equations. On the whole, we find a marginal improvement of χ^2 with our anisotropic model compared to the standard flat Λ CDM model.

We find that the energy density fractions of the anisotropic sources’ considered in this work are consistent with zero with in a 1σ confidence level. We also find that the anisotropic models considered here allow for a very small, but non-zero, shear for our universe at present times. So, a small non-zero energy density for these anisotropic sources, today, may be plausible consistent with the error bars on them, in line with the small non-zero shear today found in our anisotropic model fits to SN1a data. The data also reveals a cosmic preferred axis for our universe, independent of the anisotropic source model we used. This anisotropy axis is also found to point in roughly the same direction as some anisotropy axes found in other cosmological data that are tabulated in Table [5].

	CS	DW	LVMF	MF	Λ CDM
h_0	0.6971(31)	0.6980(30)	0.6982(30)	0.6977(31)	0.701
σ_0	0.0088(44)	0.0068(47)	0.0060(40)	0.0070(44)	-
Ω_0^{AM}	0.010(17)	0.003(33)	0.000(11)	0.0013(52)	-
Ω_0^Λ	0.730(19)	0.735(22)	0.733(24)	0.735(16)	0.734
Ω_0^{IM}	0.260(36)	0.262(55)	0.267(35)	0.264(21)	0.266
$\hat{\lambda}$	(270.21,-21.09)	(270.92,-19.12)	(269.43,-24.03)	(273.11,-19.53)	-
q_0	-0.600(37)	-0.605(66)	-0.599(41)	-0.602(27)	-0.601
χ^2	522.64	522.71	522.72	522.71	525.45
$\Delta\chi^2$	2.81	2.74	2.73	2.74	-

Table 4: Supernovae constraints on the cosmological parameters of the two models, one with an anisotropic matter source in addition to Λ CDM components in a Bianchi-I universe and, the other with only Λ CDM components in a flat FRW background, respectively. The improvement $\Delta\chi^2$ is with respect to Λ CDM model fitting (*last column*).

Axis	(l_A, b_A)
Dark Energy dipole	(309.4,-15.1)
Fine structure constant dipole	(320.5,-11.7)
Asymmetric Hubble expansion axis	(325,-19)
CMB Maximum Temperature Asymmetry axis	(331.9,-9.6)
CMB ecliptic dipole power asymmetry axis	(231,-5)
CMB Dipolar modulation axis	(218.9,-21.4)
CMB Mirror symmetry axis	(262,-14)

Table 5: Preferred directions as observed in various cosmological data plotted in Fig. [12] in addition to the anisotropy axes found in our anisotropic model (see Table [4]) are listed here [7], [21]. The axis are given in Galactic co-ordinate system.

As is evident from Fig. [12], there is a weak dependence of χ^2 on the anisotropy axis parameters $\hat{\lambda} = (l_A, b_A)$. But we find the same preferred axis for the various equation of state parameterizations corresponding to different anisotropic sources. This might be indicative of a hidden preferred axis becoming explicit, independent of the specific anisotropic parameterization used. Both the weak dependence of anisotropy axis parameters on χ^2 , and the overall improvement in χ^2 , may be remedied by a future SN1a data compilation which is homogeneous in both redshift and position spaces.

Interestingly the anisotropy axes we found here, are also approximately close to other preferred directions found in diverse cosmological data [21]. Some (three) of the other anisotropy axes seem to be lying (just) outside of the 2σ confidence level of our anisotropy axes plotted there. But they all may agree with each other in direction within that limit, as the 1σ bounds on these axes would overlap with our confidence contours (see Ref. [7] and [21] for 1σ bounds on each the anisotropy axes of Table [5]). The bottom plot of Fig. [12] shows all these diverse axes in perspective. The CMB mirror parity symmetry axis [7] is the closest one to the axes we found here, at a mere angular separation of 10° . All these axes pointing nearly in the same direction might be indicative of a cosmic preferred axis for our universe.

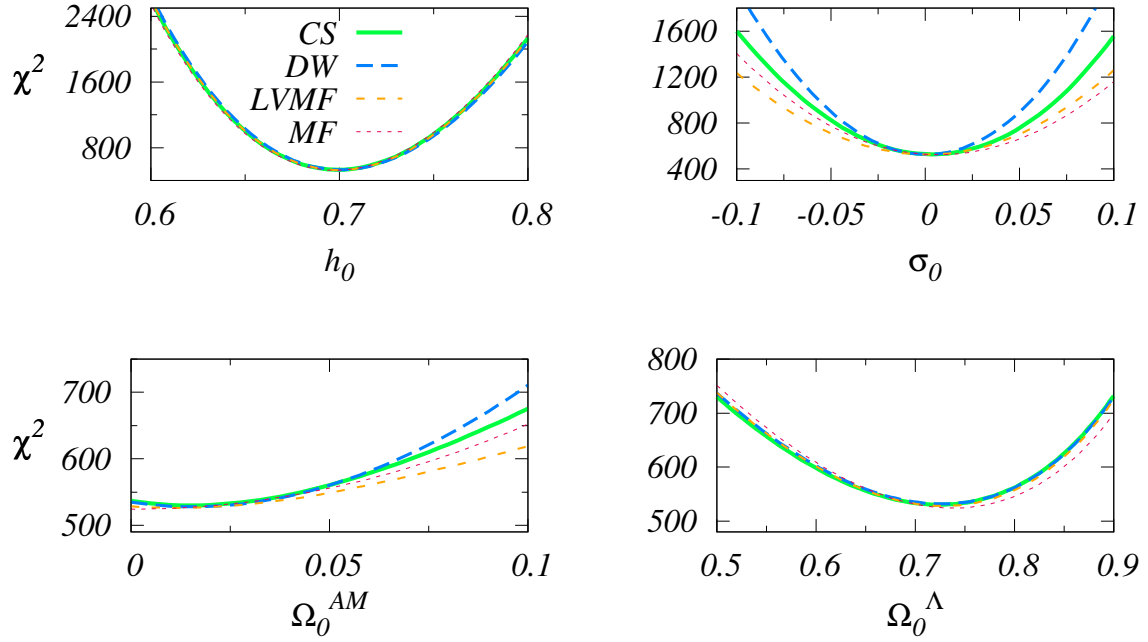


Figure 10: The behaviour of χ^2 as a function of the parameters $h_0, \sigma_0, \Omega_0^{AM}$ and Ω_0^Λ for the anisotropic universe at its minimum are shown here. Ω_0^{IM} dependence is not shown, treating it as a dependent parameter that can be estimated from the constraint equation $\Omega_{IM} = 1 - \sigma^2 - \Omega_{AM} - \Omega_\Lambda$.

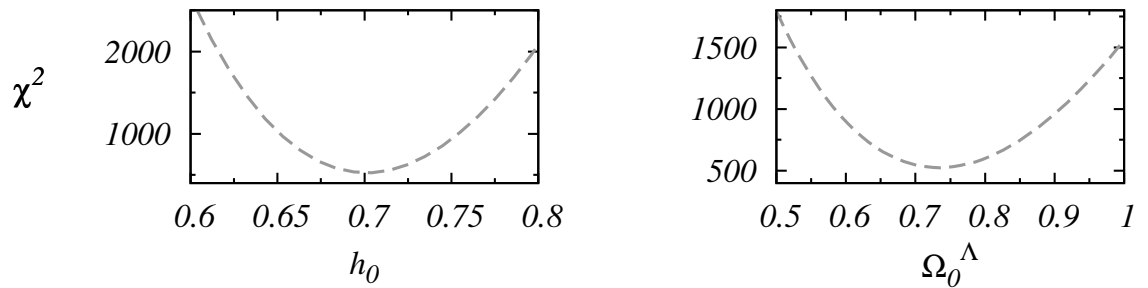


Figure 11: Same as Fig. [10], but for standard Λ CDM model parameters.

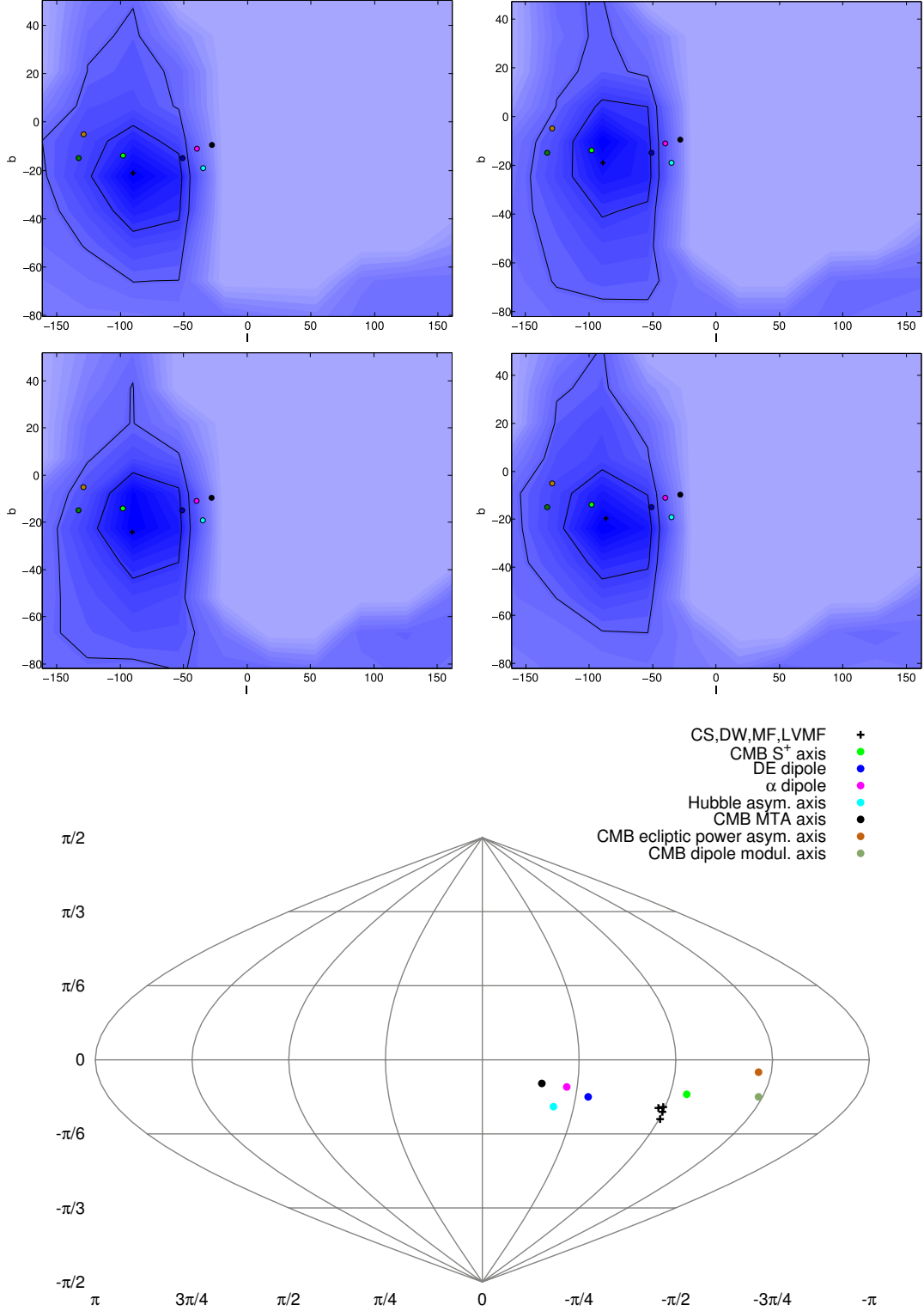


Figure 12: Plotted here are the anisotropic axes found in this work together with various anisotropic axes found in diverse cosmological observations. The reference co-ordinate system is the Galactic co-ordinate system (l, b) . The first four plots correspond to likelihoods of the anisotropic axis $\hat{\lambda} = (l_A, b_A)$ for cosmic strings, domain walls, magnetic fields and LVMF, respectively in the clockwise direction. The preferred axis specific to each of the anisotropic sources is plotted as a ‘+’, and coloured circles correspond to the other anisotropic axes. The 1σ and 2σ confidence regions are shown encompassed in black solid lines. The bottom figure shows, in perspective, all the axes on a sinusoidal projection of the celestial sky in galactic co-ordinates. These additional axes are tabulated in Table [5].

8 Conclusions

In this paper, we studied the evolution of Bianchi-I universe containing different types of anisotropic matter sources. First we analyzed the evolution of the full set of state space variables $H', h', \rho', k_0, k_1, k_2 = k_3$ in cosmic time. Depending on the initial conditions we found that there can be a sign change in the shear. This may have some interesting implications in early universe cosmology. Then we examined the evolution of dimensionless variables viz., σ, K_1 and K_3 in dimensionless time τ using dynamical systems approach. In the τ -frame, we determined the fixed points of all the evolution equations including the null geodesic equations. We also checked the stability of the fixed points numerically. We then investigated a more realistic scenario where we included isotropic dust like (dark) matter and cosmological constant as dark energy. We found that the universe asymptotically evolves to a de Sitter universe. Then, in terms of τ -time, we get an analytic expression for the temperature anisotropies of the CMBR. We generated the temperature patterns of the CMB for the four anisotropic matter sources studied here. We found that the contribution to the CMB temperature signal is mainly through the quadrupole. We also pointed out the differences between the CMB temperature maps due to these anisotropic matter types.

We then constrained the parameters of our anisotropic model using Union 2 type Ia supernova data. We found that a very small, but non-zero shear could be present today in our universe through our SN1a data constraints. A cosmic preferred axis is also found from the data for all the individual anisotropic matter source models in addition to Λ CDM components in a Bianchi-I universe. The anisotropy axes we obtained are almost same, independent of the anisotropic source we used. It turns out that this axis is very close to the mirror symmetry axis found in CMB data from Planck probe. Interestingly enough, the axes we found here coincides with the dipole axis found in a supernovae distance modulus - redshift fit to an inhomogeneous universe that does not require dark energy to explain the apparent late time acceleration of our universe [22]. So, there seems to be some evidence that we live in an anisotropic universe.

It will be interesting to generalize our results to other Bianchi classes - A and B. In case of other Bianchi models the state space would be larger and we need to find different subspace of the state space and their stable fixed points. It will also be interesting to study the CMB polarization anisotropy in these models.

Acknowledgements

S.T. would like to acknowledge Department of Science and Technology, India for financial support. We thank Santanu Das for sharing his MCMC cosmological parameter estimation code, and acknowledge the use of `CosmoLogUI`², a plotting interface to the popular `CosmoMC` output chains. We also acknowledge the use of `HEALPix`³ [23] and Eran Ofek's MATLAB routine `coco.m`⁴ for astronomical co-ordinate conversion of SN1a positions, in this work. We thank the anonymous referee for his comments which greatly helped in improving the clarity and presentation of this work.

Appendices

A Anisotropic sources

A network of domain walls can be formed during the phase transition in the early universe by spontaneous breaking of a Z_2 symmetry, separated by a distance of the order of correlation length [24]. In a self interacting real scalar field theory for a domain wall (in yz -plane), the energy momentum (e-m) tensor takes the form

$$T_{\nu}^{\mu(DW)} = A(x) \text{diag}(1, 0, 1, 1), \quad (37)$$

²<http://www.sarahbridle.net/cosmologui/>

³<http://healpix.jpl.nasa.gov/>

⁴<http://www.weizmann.ac.il/home/eofek/matlab/>

where $A(x)$ has a bell shaped distribution around $x=0$. The wall can be made thin by appropriately tuning the coupling strength and the vacuum expectation value of the self interacting scalar field.

To find the form of the e-m tensor for a network of domain walls, let us consider a collection of N planar domain walls (with walls in the yz -plane) within a box of volume V . Here we take the side of the box to be much larger than the correlation length of the vacuum expectation value of the scalar field. For this configuration e-m tensor depends on ' x ' alone. Let us assume that the walls of this stack reside at points $x^i (i = 1, 2, \dots, N)$ on the x -axis. Then the total e-m tensor for such a network of non-interacting walls is given by

$$T_{\nu}^{\mu} = \sum_{i=1}^N T_{\nu}^{\mu(DW)}(x^i - x). \quad (38)$$

In the case of a large N , we can have a function $g(x)$ which is the average number of walls per unit length in the range x and $x + dx$. It is normalized to satisfy $\int g(x)dx = N$. Then the average e-m tensor of this configuration is given by

$$\langle T_{\nu}^{\mu} \rangle = \frac{\int dx \int dx' g(x') T_{\nu}^{\mu(DM)\mu}(x - x')}{\int g(x)dx}. \quad (39)$$

With an average distance between the walls as ' d ', we can approximate the average e-m tensor as

$$\langle T_{\nu}^{\mu} \rangle \simeq \frac{1}{d} D_{\nu}^{\mu}, \quad (40)$$

where $D_{\nu}^{\mu} = \text{diag}(\eta, 0, \eta, \eta)$ and $\eta = \int A(x) dx$ is the surface energy density.

Now we can use appropriate Lorentz transformation to get the e-m tensor for the case when domain walls are moving in the x -direction with an average velocity β . In this case D_{ν}^{μ} becomes

$$D_{\nu}^{\mu} = \begin{pmatrix} \gamma^2 \eta & -\gamma^2 \beta \eta & 0 & 0 \\ -\gamma^2 \beta \eta & \gamma^2 \beta^2 \eta & 0 & 0 \\ 0 & 0 & \eta & 0 \\ 0 & 0 & 0 & \eta \end{pmatrix} \quad (41)$$

where $\gamma = \sqrt{1 - \beta^2}$. For slowly moving domain walls, e-m tensor can be approximated by

$$\langle T_{\nu}^{\mu} \rangle \simeq \frac{1}{d} \text{diag}(\eta, 0, \eta, \eta). \quad (42)$$

Such a network of slowly moving domain walls may be present now, for example, due to an interaction of dark matter with the domain walls [25]. Distortion of the cosmic microwave background is negligible in that toy model. This network of stacked non-relativistic domain walls can be described as a perfect fluid with equation of state $p = (p_a + 2p_b)/3 = -\frac{2}{3d}\eta$.

Similarly, it is well known that a network of cosmic strings can be formed during the phase transition in the early universe when a U(1) symmetry is broken. The e-m tensor due to an infinite string with mass per unit length μ along the x -direction is given by [24]

$$T_{\nu}^{\mu(CS)} = \mu \delta(y) \delta(z) \text{diag}(1, 1, 0, 0). \quad (43)$$

Analogous to our construction of domain wall network one can easily construct the average e-m tensor for a network of slowly moving cosmic strings along a particular direction which can be approximated by

$$T_{\nu}^{\mu} \simeq \frac{1}{d^2} \text{diag}(\mu, \mu, 0, 0), \quad (44)$$

where d is the average separation between the cosmic strings. Such a network of non-relativistic cosmic strings can be described as a perfect fluid with an equation of state $p = (p_a + 2p_b)/3 = -\frac{1}{3d^2}\mu$.

The actual evolution of cosmic string and domain wall networks are complicated. In this paper, we do not consider the nonlinear evolution of these networks with effects such as formation of intersection and loops, and any gravitational effects such as collapse and emission of gravitational radiation.

	σ_0	g	
	1	2	U
CS	-1	6	U
	1/2	-3/2	S
	1	7	U
DW	-1	3	U
	-2/5	-21/10	S
	1	4	U
LVMF	-1	0	S
	-1	0	S
	1	-2	S
MF	-1	6	U
	2	3	U

Table 6: The full list of fixed points for the shear parameter, σ , are shown here, pointing out the stable (S) and unstable (U) values. Here ‘ g ’ corresponds to the constant coefficient in equation $\frac{d\Delta\sigma}{d\tau} = g \Delta\sigma$ from Eq. [45].

	σ_0	K_1^0	K_2^0	γ_1	γ_2	γ_3	
CS	1/2	± 1	0	-3/2	-3	-3/2	S
		0	$\pm 1/\sqrt{2}$	-3/2	3/2	0	U
DW	-2/5	± 1	0	-21/10	12/5	6/5	U
		0	$\pm 1/\sqrt{2}$	-21/10	-6/5	0	S
LVMF	-1	± 1	0	0	6	3	U
		0	$\pm 1/\sqrt{2}$	0	-3	0	S
MF	1	± 1	0	-2	-6	-3	S
		0	$\pm 1/\sqrt{2}$	-2	3	0	U

Table 7: The full list of fixed points corresponding to the set of equations Eq. [45] is shown here. In the last column, an ‘S’ denotes a stable fixed point and ‘U’ denotes an unstable fixed point.

B Stability analysis

Let us denote σ_0, K_1^0 and K_2^0 to be the fixed points of Eq. [11], [12] and [14]. Let us consider perturbations around these fixed points as $\sigma_0 + \Delta\sigma, K_1^0 + \Delta K_1$ and $K_2^0 + \Delta K_2$. Keeping terms only upto first order in perturbation, we get

$$\frac{d}{d\tau} \begin{bmatrix} \Delta\sigma \\ \Delta K_1 \\ \Delta K_2 \end{bmatrix} = \begin{bmatrix} -\frac{3}{2}(1-w)(1-3\sigma_0^2) + 2(w_a - w_b)\sigma_0 & 0 & 0 \\ 3(1-(K_1^0)^2)K_1^0 & 3(1-3(K_1^0)^2)\sigma_0 & 0 \\ -3(K_1^0)^2 K_2^0 & -6K_1^0 K_2^0 \sigma_0 & -3(K_1^0)^2 \sigma_0 \end{bmatrix} \begin{bmatrix} \Delta\sigma \\ \Delta K_1 \\ \Delta K_2 \end{bmatrix}. \quad (45)$$

The three eigenvalues of the above matrix equation viz., $\gamma_1, \gamma_2, \gamma_3$ are given by

$$\begin{aligned} \gamma_1 &= -\frac{3}{2}(1-w)(1-3\sigma_0^2) + 2(w_a - w_b)\sigma_0 \\ \gamma_2 &= 3(1-3(K_1^0)^2)\sigma_0 \\ \gamma_3 &= -3(K_1^0)^2 \sigma_0. \end{aligned} \quad (46)$$

These eigenvalues determine whether a fixed point is stable or unstable. For the shear parameter, σ , all possible fixed points are listed in Table [6], and the complete list of fixed points of K_i , as dictated by the eigenvalues γ_1, γ_2 and γ_3 , are given in Table [7].

References

- [1] Fixsen D. J. et al., 1996, ApJ, 473, 576; Bennett C. L. et al., 2003, ApJS, 148, 1
- [2] Ehlers J., Geren P. and Sachs R. K., 1968, Jour. Math. Phys, 9, 1344

- [3] Stoeger W. R., Maartens R. and Ellis G. F. R., 1995, ApJ, 443, 1
- [4] Hinshaw G. et al., 2003, ApJS, 148, 135; Efstathiou G., 2003, MNRAS, 346, L26; Tegmark M., de Oliveira-Costa A. and Hamilton A. J., 2003, Phys. Rev. D, 68, 123523; de Oliveira-Costa A. et al., 2004, Phys. Rev. D, 69, 063516; Ralston J. P. and Jain P., 2004, Int. Jour. Mod. Phys. D, 13, 1857; Schwarz D. J. et al., 2004, Phys. Rev. Lett. 93, 221301; Eriksen H. K. et al., 2004, ApJ, 605, 14; Hansen F. K. et al., 2009, ApJ, 704, 1448; Hanson D. and Lewis A., 2009, Phys. Rev. D, 80, 063004; Land K. and Magueijo J., 2005, Phys. Rev. D, 72, 101302; Kim J. and Naselsky P., 2010, Phys. Rev. D, 82, 063002; Aluri P. K. and Jain P., 2012, MNRAS, 419, 3378; Spergel D. N. et al., 2003, ApJS, 148, 175; Copi C. et al., 2007, Phys. Rev. D, 75, 023507; Vielva P. et. al., 2004, ApJ, 609, 22
- [5] Berera A., Buniy R. V. and Kephart T. W., 2004, JCAP, 10, 16; Slosar A. and Seljak U., 2004, Phys. Rev. D, 70, 083002; Gordon C. et al., 2005, Phys. Rev. D, 72, 103002; Moffat J. W., 2005, JCAP, 10, 12; Buniy R. V., Berera A. and Kephart T. W., 2006, Phys. Rev. D, 73, 063529; Ackerman L., Carroll S. M. and Wise M. B., 2007, Phys. Rev. D, 75, 083502; Bunn E. F. and Bourdon A., 2008, Phys. Rev. D, 78, 123509; Aluri P. K. et. al., 2010, MNRAS, 41, 1032; Efstathiou G., Ma Y-Z. and Hanson D., 2010, MNRAS, 407, 2530; Aurich R. and Lustig S., 2011, MNRAS, 411, 124; Copi C. J. et al., 2011, MNRAS, 418, 505; Feeney S. M., Peiris H. V. and Pontzen A., 2011, Phys. Rev. D, 84, 103002; Sung R., Short J. and Coles P., 2011, MNRAS, 412, 492; Aluri P. K. and Jain P., 2012, Mod. Phys. Lett. A, 27, 1250014
- [6] Bennett C. et.al., 2011, ApJS, 192, 17
- [7] Ade P. A. R. et al. [Planck Collaboration], Planck 2013 results - XXIII, arXiv:1303.5083
- [8] Gumrukuoglu A. E., Contaldi C. R. and Peloso M., 2007, JCAP, 11, 005; Pereira T. S., Pitrou C. and Uzan J.-P., 2007, JCAP, 09, 006; Pitrou C., Pereira T. S. and Uzan J.-P., 2008, JCAP, 04, 004; Watanabe M.-a., Kanno S. and Soda J., 2009, Phys. Rev. Lett., 102, 191302
- [9] Campanelli L., Cea P. and Tedesco L., 2006, Phys. Rev. Lett., 97, 131302; Campanelli L., Cea P. and Tedesco L., 2007, Phys. Rev. D, 76, 063007
- [10] Barrow J. D., 1997, Phys. Rev. D, 55, 7451; Barrow J. D., Ferreira P. G. and Silk J., 1997, Phys. Rev. Lett., 78, 3610; Barrow J. D., arXiv:gr-qc/9712020; Barrow J. D. and Maartens R., 1999, Phys. Rev. D, 59, 043502
- [11] Koivisto T. and Mota D., 2008, JCAP, 06, 018; Campanelli L., Cea P., Fogli G. L. and Marrone A., 2011, Phys. Rev. D, 83, 103503
- [12] Campanelli L., 2009, Phys. Rev. D, 80, 063006
- [13] Thorsrud M., Mota D. F. and Hervik S., 2012, JHEP, 10, 066
- [14] Wainwright J. and Ellis G. F. R., 1997, *Dynamical systems in cosmology*, Cambridge University Press
- [15] Ellis G. F. R. and MacCallum M. A. H., 1969, Comm. Math. Phys., 12, 108
- [16] Nilsson U. S., Ugglä C. and Wainwright J., 2000, Gen. Rel. Grav., 32, 1319
- [17] Calogero S. and Heinzle J. M., 2011, Physica D, 240, 636
- [18] Lim W. C., Nilsson U. S. and Wainwright J., 2001, Class. Quant. Grav., 18, 5583
- [19] Alnes H. and Amarzguioui M., 2006, Phys. Rev. D, 74, 103520
- [20] Hamuy M., Phillips M. M., Suntzeff N. B., Schommer R. A. and Maza J., 1996, Astron. J., 112, 2408; Blakeslee J. P. et al., 2003, ApJ, 589, 693; Tonry L. et al., 2003, ApJ, 594, 1; Barris B. J. et al., 2004, ApJ, 602, 571; Riess A. G. et al., 2004, ApJ, 607, 665; Krisciunas K. et al., 2005,

Astron. J., 130, 2453; Astier P. et al., 2006, A&A, 447, 31; Jha S., Riess A. G. and Kirshner R. P., 2007, ApJ, 659, 122; Miknaitis G. et al., 2007, ApJ 666, 674; Riess A. et. al., 2007, ApJ, 659, 98; Kowalski, M. et al., 2008, ApJ, 686, 749

[21] Webb J. K. et al., 2011, Phys. Rev. Lett., 107, 191101; Mariano A. and Perivolaropoulos L., 2012, Phys. Rev. D, 86, 083517; Kalus B., Schwarz D. J., Seikel M. and Wiegand A., 2013, A&A, 553, A56; Mariano A. and Perivolaropoulos L., 2013, Phys. Rev. D, 87, 043511

[22] Alnes H. and Amarzguioui M., 2007, Phys. Rev. D75, 023506

[23] Gorski K. M. et al., 2005, ApJ, 622, 759

[24] Kolb E. W. and Turner M. S., 1994, *The Early Universe*, Westview Press; Vilenkin A. and Shellard E. P. S., 2000, *Cosmic Strings and other Topological Defects*, Cambridge University Press

[25] Massarotti A., 1991, Phys. Rev. D, 43, 2, 346